DESY Zeuthen Summer Student Program 2011

Investigation of Leptonic Models for Very High Energy Radiation from Supernova Remnants

Astroparticle Physics

Author: Nina Kudryashova

Supervisor: Dr. Rebecca Gozzini

1 Introduction

The discovery of the cosmic rays in 1911 by Victor Hess was the birth of modern particle astrophysics. Since learning that the Earth is constantly being bombarded by particles coming from outside the terrestrial atmosphere, we have uncovered a lot about their origins. Charged cosmic rays are composed of about 86% protons, 11% ionized helium nuclei and 2% electrons, with the remainder attributed to heavier elements [12]. It is clear today that most of the charged particles in cosmic rays come from outside the solar system and that they are accelerated through different processes. However, the exact mechanisms of cosmic rays' production are still unclear. The energy spectrum of cosmic rays observed at Earth (figure 1) spans many orders of magnitude and has two distinct features: the knee and the ankle, where the index of the power law fit to the spectrum changes.

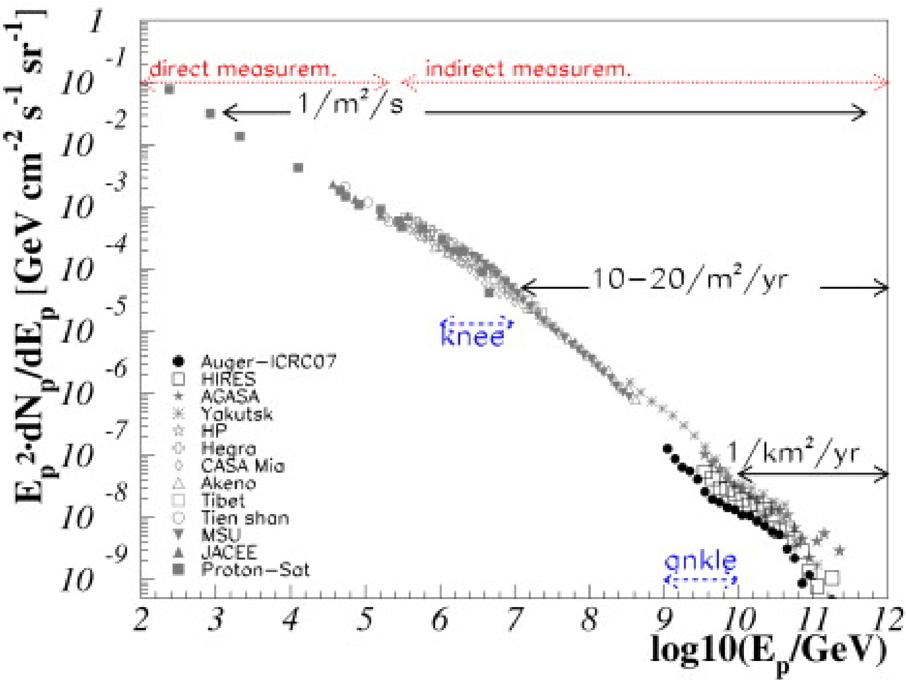

Figure 1: Cosmic rays spectrum as observed by various ground-based and atmospheric telescopes. Image courtesy of J.K. Becker [5].

It is believed that most cosmic rays past the knee are of an extragalactic origin, and are supposedly produced in large part by Gamma Ray Bursts and Active Galactic Nuclei. Cosmic rays up to the knee ($\sim 10^{15}$ eV) are believed to be originating within our galaxy and their main progenitors are generally accepted to be supernova remnants (SNRs) [12]. The initial reasoning behind this conjecture was the fact that the energy density in cosmic rays combined with their lifetime in the galaxy had to be maintained by a power source with a similar energy output to SNRs. A suitable galactic acceleration mechanism was first proposed by Enrico Fermi in 1949 [9]. It was later applied to SNRs and is referred to as diffusive shock acceleration (see eg. [6]). In essence, particles (be it electrons, protons or nuclei) are trapped between a shock front and a region of high magnetic fields, and are accelerated by crossing the shock boundary back and forth, resulting in a net gain of energy. Figure 2 illustrates the simplest version of this process. Diffusive shock acceleration can have different timescales depending on the initial energies of the ejected particles, but the resulting particle spectrum is a power law with an index depending solely on the shock compression ratio.

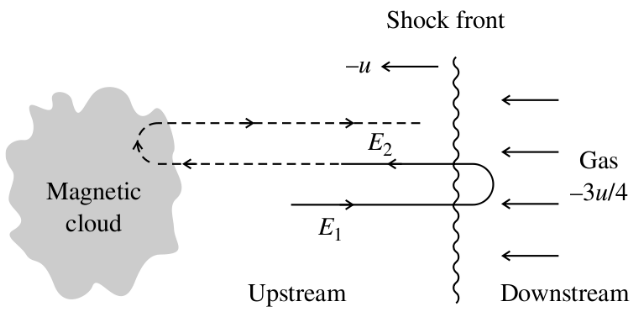

Figure 2: Schematic representation of diffusive shock acceleration. Image courtesy of D. Perkins ([12]).

Apart from possessing a suitable acceleration mechanism, SNRs are often surrounded by a molecular cloud providing the acceleration population. Furthermore, since this work only considers galactic sources (i.e. relatively close ones), absorption of cosmic rays on their way to Earth is negligible.

2 Theoretical background

2.1 Supernova Remnants

Supernova remnants are the remains of a dead star that underwent a supernova explosion for one of the following reasons: either it burned through its internal fuel supply and reached an iron core, resulting in a gravitational core collapse; or it was a white dwarf that accumulated mass on its surface past the Chandrasekhar limit, resulting in a thermonuclear explosion; or it was a binary degenerate dwarf system that underwent a merging and immediately overcame the Chandrasekhar limit, also exploding. In either case, the explosion creates a shock wave propagating into the surrounding medium and sweeping up any matter on its way, accelerating particles through the diffusive shock acceleration mechanism. SNRs are often divided into three types according to their topology. Shell type make up $\sim 80\%$ of all galactic remnants and have a uniform emission from the shell region. Plerionic (or Crab-like) have an increasing emittance as one moves towards the central region. It is now believed that they contain a compact object (often a pulsar) in its center and make up $\lesssim 10\%$ of galactic remnants. They are also referred to as Pulsar Wind Nebulae, or PWN. Composite (or mixed morphology) are shell-like containing a PWN. For the purpose of this work, only shell type SNRs are considered, as they constitute the bulk of galactic SNRs. Furthermore, all SNRs undergo distinctive evolution phases as they age. The break down of those phases can be summarizes as:

- ⋆ **Free expansion** lasts approximately until the SNR has swept up its own mass in circumstellar material, which is usually on the order of a hundred years.

- ⋆ **Sedov phase** is an adiabatic expansion of the blast wave where the expansion starts to slow down and the turbulent magnetic fields within the remnant accelerate particle populations. This phase lasts on the order of 10000 years.

- ⋆ **Radiative snow-plow** refers to the remnant becoming more transparent to optical photons, as electrons are being captured by protons and ions. Expansion velocity slows down significantly over the next tens of thousands of years.
- ⋆ **Dispersion** occurs as the SNR starts merging with the interstellar medium and radiates mostly in the thermal regime.

For the purpose of particle acceleration, the key phase is Sedov. The bulk of SNR cosmic rays comes from this phase, and so do the subsequently produced gamma rays [8]. Thus, when looking for high-energy gamma ray potential sources, is it crucial to identify the evolution stage of a given remnant.

2.2 Gamma ray production mechanisms

Accelerated particles produce photons of different energies through various radiation mechanisms. In the radio range for instance, it is commonly agreed that most detected photons are due to synchrotron radiation. In the gamma ray range (corresponding to energies above approximately 1 MeV), the main production mechanism is still being disputed. Potential candidates can be divided into two main categories: hadronic and leptonic processes. In the first case, the interaction is governed by strong force and thus accessible only to hadrons (in this case mostly protons). Leptonic processes considered are governed by the electromagnetic force, and concern mostly electron populations[1]. The three main production mechanisms are:

- ⋆ π^0 **decay**, a hadronic process in which p-p interaction leads to π^0 production and its subsequent decay into two high energy γ's. This process is strongly dependent on the presence of proton populations and furthermore cannot occur in the absence of surrounding medium.
- ⋆ **Inverse Compton scattering (IC)**, a leptonic process in which a high energy electron transfers energy to a much colder photon. IC is the only process that needs no surrounding medium, as it always occurs on the cosmic microwave background and sometimes on infrared emission from gas clouds, if they are present.
- ⋆ **Bremsstrahlung (braking radiation)**, a leptonic process in which a high-energy electron interacts with the colder surrounding medium (be it other electrons, protons or heavier ions) and a high energy photon is emitted as a result. Note that like π^0 decay, the surrounding medium is crucial, but its composition need not be hadronic.

This work is mostly concerned with the Bremsstrahlung radiation and seeks to explore a lepton-dominated production scenario of observed γ-ray fluxes from SNRs. A comparison between relative scales of Bremsstrahlung and Inverse Compton radiation is also given.

2.3 Bremsstrahlung

Bremsstrahlung is the process occurring when one charged particle scatters on another one, losing some of its kinetic energy in the form of an emitted photon. Figure 3 demonstrates the four possible Feynman diagrams for the process.

[1] The designation "leptonic" should not be understood as "possible only for leptons", but rather as "dominated by leptons", since protons can also interact through both presented processes, albeit radiating significantly less efficiently than electrons.

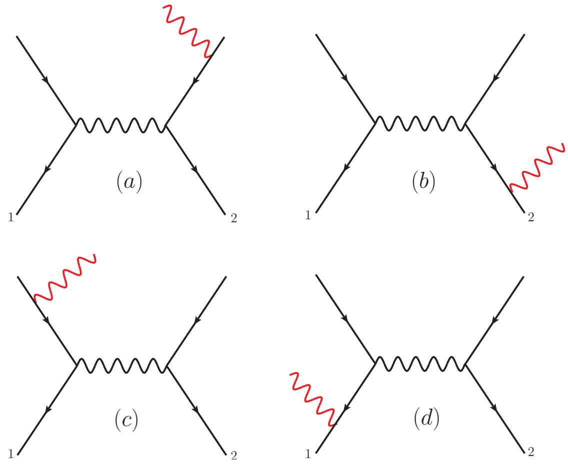

Figure 3: Feynman diagrams for e-e or e-p Bremsstrahlung. Figure reproduced from Blumenthal & Gould, 1970 [7].

In the figure, time is flowing from top to bottom, and numbers 1 and 2 correspond to the target particle and the incoming one respectively. For the case of high energy electrons scattering on the circumstellar medium, particle 1 is initially at rest (or practically so) and particle 2 is very energetic. Since we are mostly interested in the high energy Bremsstrahlung photons, only diagrams (a) and (b) contribute significantly to the effective cross-section. This is due to the fact that a system with low momentum cannot emit a very energetic photon (such as a gamma ray). The cross-section for the interaction is taken from [4] and is given by

$$\sigma(\gamma_e, \epsilon_\gamma) = \frac{4r_0^2\alpha}{\epsilon_\gamma}\left[1 + \left(\frac{1}{3} - \frac{\epsilon_\gamma}{\gamma_e}\right)\left(1 - \frac{\epsilon_\gamma}{\gamma_e}\right)\right]\left[\log\left(2\gamma_e\frac{\gamma_e - \epsilon_\gamma}{\epsilon_\gamma}\right) - \frac{1}{2}\right],$$

where r_0 is the classical electron radius, α is the fine structure constant, ϵ_γ is the resulting photons' energy in units of $m_e c^2$, and γ_e is the electron Lorentz factor. At the highly relativistic energies we consider, the difference between e-e and e-p Bremsstrahlung cross-sections is negligible, and thus σ is used for both target populations. The resulting photon emittance at source is obtained by folding the cross section with the original electron distribution and scaling it by the density of the target medium (in this case, either electrons or protons). We obtain:

$$\frac{dQ_\gamma}{d\epsilon_\gamma} = (n_e + n_p)\int_{\gamma_1}^{\gamma_2} d\gamma_e \sigma(\gamma_e, \epsilon_\gamma) N_e(\gamma_e), \tag{1}$$

where n_e and n_p are the electron and proton target densities respectively. The above expression yields the photon spectrum at source assuming a point-like emitter. To get the observed photon spectrum at Earth, $\frac{dN_\gamma}{d\epsilon_\gamma}$, one scales equation 1 by $4\pi d^2$, where d is the distance to the source. For an extended source, one further scales by the source effective area. Furthermore, an overall normalization (corresponding to the total number of emitted particles) is a flexible parameter usually fixed by fitting to the observational data.

3 MAGIC Telescope

The two main types of telescopes for γ-ray observation are ground based and space based. The best known current space based telescope is Fermi LAT, which is detecting gamma rays using pair-production and subsequent medium ionization. Ground based telescopes mostly use the Cherenkov radiation produced by an ultrarelativistic particle cascade that originated when a gamma ray interacted with the atmosphere. Cherenkov light then hits the telescope mirrors and passes through photomultipliers, permitting for reconstruction of the direction and energy of the progenitor particle. This is also the principle behind the Major Atmospheric Gamma-ray Imaging Cherenkov telescope, or MAGIC. The observatory is situated on La Palma, one of the Canary Islands, at an altitude of about 2200 meters. MAGIC is sensitive to photon energies between 50 GeV and 30 TeV, making it complementary to Fermi LAT (sensitive to maximal energies on the order of 100 GeV). It should be noted that VERITAS (Very Energetic Radiation Imaging Telescope Array System) covers approximately the same energy range as MAGIC, and the two can thus be used to cross-check each other. The third similar telescope is H.E.S.S. (High Energy Stereoscopic System), which covers a similar energy range, but has its best visibility in a different part of the sky than MAGIC and VERITAS. MAGIC is situated at a latitude of 28.8° and can observe objects at an inclination of about 60° in each direction from the vertical. This field of view covers most of the sky as shown in figure 4.

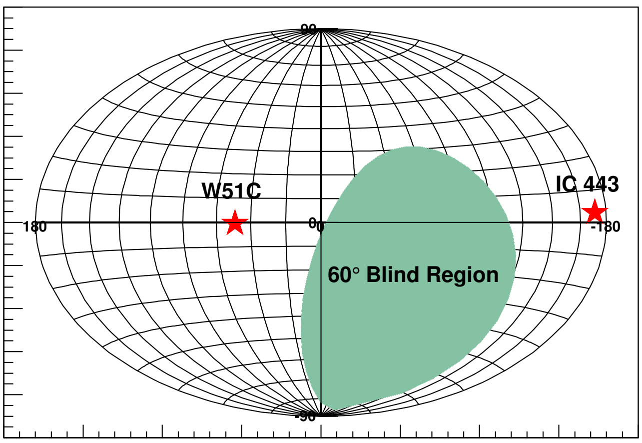

Figure 4: Aitoff-Hammer projection of the galactic skymap with MAGIC 60° field of view and two SNRs it detected.

The data obtained by MAGIC is often converted to one of the following formats: a light curve, which is a temporal evolution of the source intensity, or an SED (spectral energy distribution) curve, representing energy density emitted per second per area. Because SNRs are not variable sources, this work only includes SEDs, given as $E_\gamma^2 \frac{dN_\gamma}{dE_\gamma}$ vs E_γ.

4 Results

4.1 Method

The model used for the original electron population is a smoothed out broken power law used by the Fermi collaboration to fit some of their SNR data [1]. It is given by:

$$N_{e^-} = \left(\frac{E}{E_0}\right)^{-s}\left(1+\left(\frac{E}{E_{br}}\right)^2\right)^{-\frac{\Delta s}{2}}, \tag{2}$$

where E_0 is 1 GeV and E_{br} is the spectrum break energy, determined from observations and usually lying within 1-10 GeV. It should be noted that a broken power law model was not originally motivated by the physics of particle acceleration, but started out as a purely fitting construct, used for cases when a power law with a cutoff gives a disastrous fit. However, some recent models do yield this type of spectrum (see eg [10]) for middle-aged SNRs. The adjustable parameters in equation 2 are s, Δs and E_{br}. The first is somewhat fixed by observations in the X-ray parts of the electromagnetic spectrum, due to photons originating from the synchrotron radiation. However, this also warrants further investigation, as the synchrotron spectrum has another free parameter that may relax the constraints on s, the magnetic field strength. The other two parameters may be varied within reason to explore different dominating production mechanisms. Once those two are fixed, the IC spectrum is completely determined (up to the overall normalization), but the Bremsstrahlung one still has an extra degree of freedom, the density of the surrounding medium. The relative photon energy density spectra can thus be compared for different target density. This is further discussed in section 4.3.

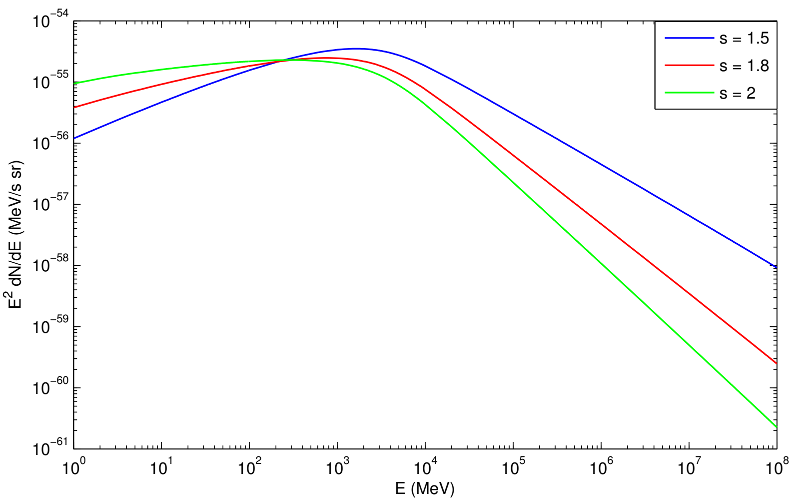

Figure 5: Non-normalized Bremsstrahlung radiation energy spectrum from electron population with varying first spectral index.

To get an intuitive feeling for the implemented Bremsstrahlung model, several energy spectra were produced with varying parameters. For instance, varying s, the first spectral index, affected both parts of the resulting spectrum (before and after the break) as can be seen in figure 5. We can conclude that this parameter cannot be varied freely to fit data past the break, as it would change the fit before the break as well. This can be contrasted with the role of Δs in the overall shape of the spectrum. As is obvious from figure 6, changing this parameter affects solely the spectral shape after the break, resulting in greater freedom during fitting.

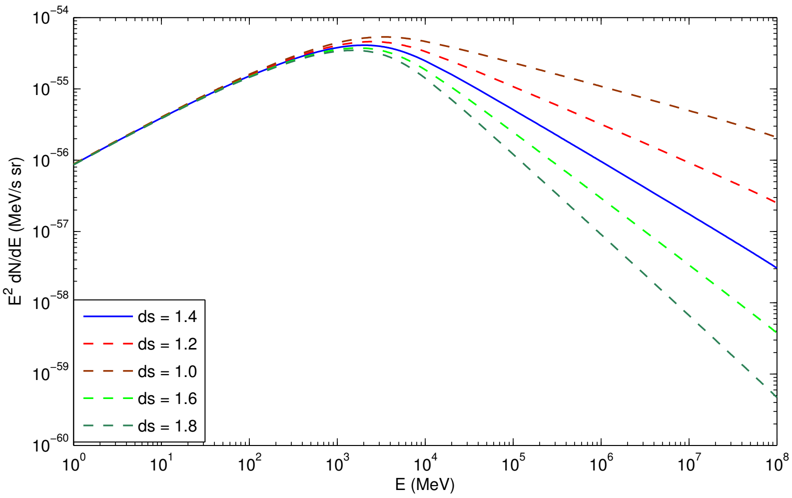

Figure 6: Non-normalized Bremsstrahlung radiation energy spectrum from electron population with varying second spectral index.

4.2 Data fitting

As an example of Bremsstrahlung dominated fits to the gamma ray part of the SNR energy spectra, the cases of W51C and IC443 SNRs were taken. They were chosen because both Fermi LAT and MAGIC data was available, making it possible to fit a larger gamma-ray energy interval. The electron spectral parameters for both fits are listed in the table 1.

Table 1: Fitting parameters for the electron distribution

Fit	Parameter	W51	IC443
Fermi	s	1.5	1.93
	Δs	1.4	0.63
	E_{br} (MeV)	5000	3250
Bremsstrahlung optimized	s	1.5	1.9
	Δs	1.32	1.1
	E_{br} (MeV)	5000	10000

First, a Bremsstrahlung spectrum was computed using the optimal Fermi collaboration fit parameters (determined from their observations as well as from the synchrotron-dominated region). Those parameters, along with the Fermi LAT data points were taken from [1] and [2] for W51C and IC443 respectively. The MAGIC data was taken from [11] and [3] respectively. Then, a Bremsstrahlung-optimized fit was done, without changing the first spectral index as quoted by the Fermi Collaboration (to avoid affecting the fit before the break)[2]. The results are presented in figure 7 where W51C is at the top and IC 443 at the below.

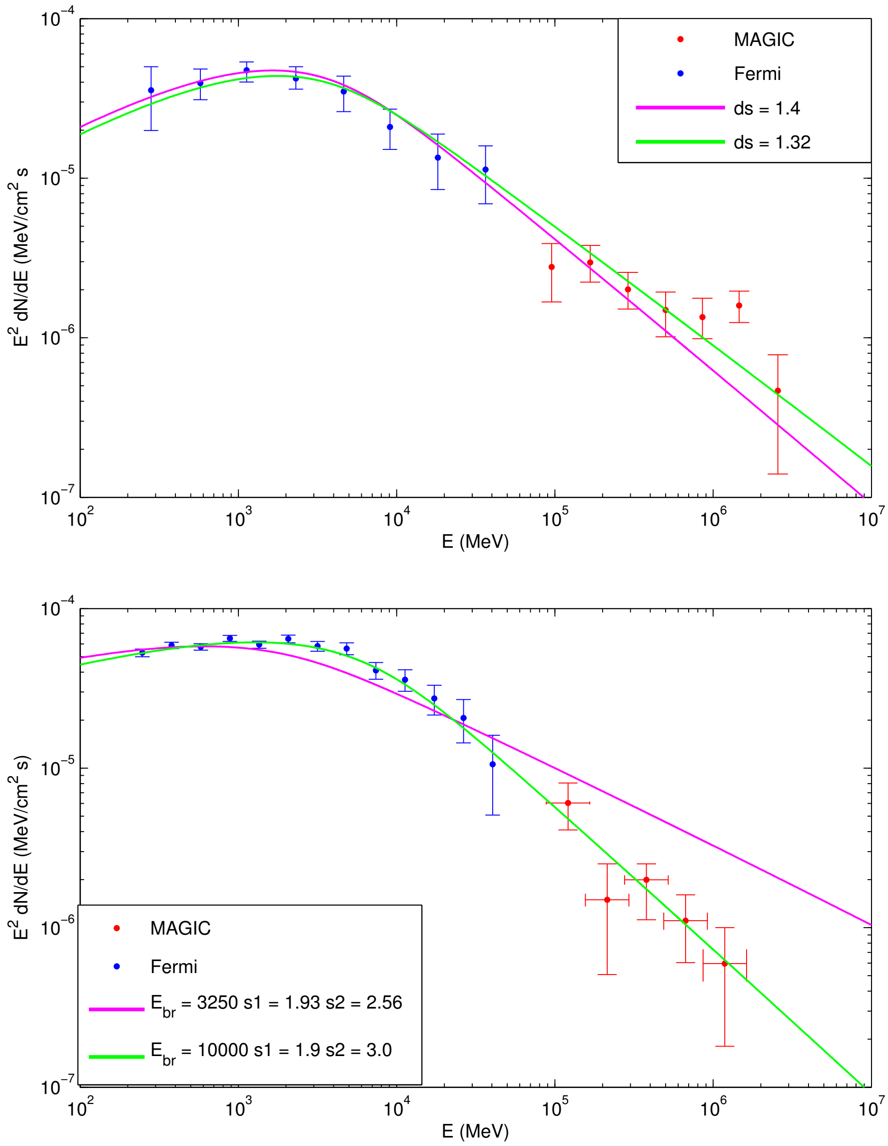

Figure 7: Observed energy density spectrum of SNRs W51C (above) and IC 443 (below) with corresponding Fermi parameters (pink) and Bremsstrahlung-optimized (green) fits.

Comparing the two data fits, one observes the following. W51C gives a much better Bremsstrahlung-optimized fit for the original Fermi parameters than IC 443. For the latter, the break energy had to be significantly adjusted to obtain a reasonable Bremsstrahlung fit. Increasing the break energy affects the synchrotron part of the photon energy spectrum, but it is likely that any change would manifest itself past the data. This assumption, however, was not thoroughly checked due to time limitations.

[2]In the case of IC443, the first index was changed within the quoted error

4.3 Inverse Compton and Bremsstrahlung comparison

As mentioned previously, a photon spectrum from Inverse Compton is completely determined by the initial electron spectrum, as well as the scattering photon population(s). Once these parameters are fixed, only the overall normalization can be adjusted. This is not the case for Bremsstrahlung, where the densities of the target particles' populations are crucial to the relative height of the spectrum. Thus, Bremsstrahlung spectrum can be adjusted relative to the Inverse Compton one within reasonable values of target densities. Figure 8 illustrates this for Inverse Compton from Cosmic Microwave Background photons compared to Bremsstrahlung spectra for three different medium densities. The parameters for both fits are given in table 2.

Table 2: Parameters for IC and Bremsstrahlung SED comparison

Parameter	Value
s	1.5
Δs	1.4
E_{br}	10^{10} eV
E_0	10^{10} eV

The IC spectrum should not be taken too literally, as it does not contain contribution from infrared and optical photon populations that may be present. This can be computed in the future using GALPROP, or a similar software. A full IC spectrum would have its peak shifted to the right (since infrared and optical photons are more energetic than the CMB ones) and would be overall higher, most likely comparable to Bremsstrahlung at densities 1-10 particles/cm^3. The slopes of Bremsstrahlung and IC spectra are slightly different for the same parameter values, also leading to more flexibility while fitting the data using one or the other.

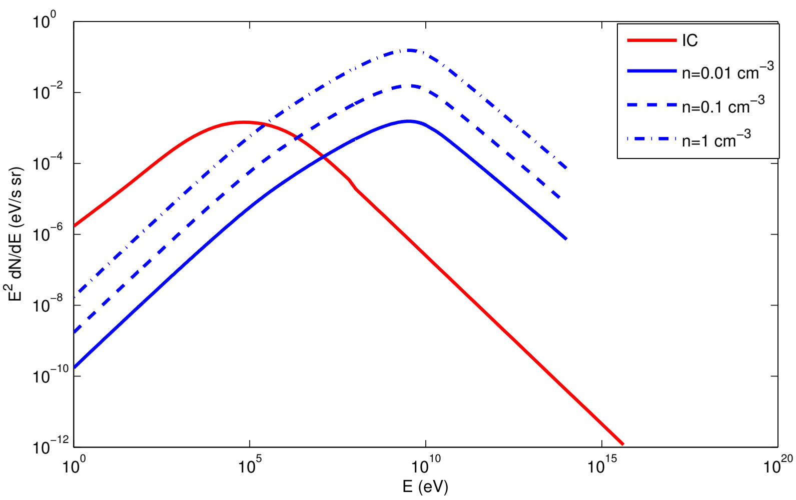

Figure 8: Relative SED of the Bremsstrahlung and Inverse Compton from CMB spectra for various target medium densities. IC spectrum courtesy of Fabian Jankowski.

5 Conclusion

To conclude, a Bremsstrahlung-dominated scenario of gamma ray production is plausible with reasonable parameters. Further investigation will be needed to say whether such a scenario would be able to reproduce observations over the whole data range. Furthermore, it is now clear that the Bremsstrahlung and IC relative heights can be adjusted while fitting, due to the extra free parameter (medium density) going into the latter. A potential future endeavor can be determining what sort of parameters would lead to a comparable contribution from Bremsstrahlung and IC, which could be used to model non-linearities in the data. The question of whether leptonic models can ever dominate over the hadronic one still remains open, as the former requires large electron populations, and the latter large proton ones, and determining those populations at source is not trivial.

6 Aknowledgments

First, I am very grateful to Dr. Christian Spiering, who accepted me into the Particle Astrophysics group at DESY Zeuthen, thus enabling this work. Furthermore, I would like to express my sincere gratitude to my supervisor, Dr. Rebecca Gozzini, who is not only an excellent mentor, but a great personal inspiration. This work could not be achieved without her constant support and guidance. I would further like to thank Fabian Jankowski for his valuable discussions and for providing the data for the Inverse Compton simulations. Also, I wish to thank my father for his valuable comments concerning this work. I am also very grateful to Dr. Karl Jansen, for being the best super-supervisor to all the summer students and for his omnipresent cheerfulness. Finally, I thank all the summer students for an amazing experience at the DESY Summer School 2011.

7 References

References

[1] A.A. Abdo et al., *Fermi LAT Discovery of Extended Gamma-Ray Emission in the Direction of Supernova Remnant W51C*, The Astrophysical Journal Letters, **706** (2009), L1.

[2] A.A Abdo et al., *Observation of Supernova Remnant IC 443 with the Fermi Large Area Telescope*, The Astrophysical Journal, **712** (2010), 459.

[3] J. Albert et al., *Discovery of VHE Gamma Radiation from IC 443 with the MAGIC Telescope*, The Astrophysical Journal Letters, **664** (2007), L87.

[4] M.G. Baring, D.C. Ellison, S. P. Reynolds, I. A. Grenier, and P. Goret, *Radio to Gamma-Ray Emission from Shell-Type Supernova Remnants: Predictions from Non-linear Shock Acceleration Models*, The Astrophysical Journal, **513** (1999), 311.

[5] J.K. Becker, *High-energy neutrinos in the context of multimessenger astrophysics*, Physics Reports, **458** (2008), no. 4-5, 173 – 246.

[6] E.G. Berezhko and D.C. Ellison, *A Simple Model of Nonlinear Diffusive Shock Acceleration*, The Astrophysical Journal, **526** (1999), 385.

[7] G.R. Blumenthal and R.J. Gould, *Bremsstrahlung, Synchrotron Radiation, and Compton Scattering of High-Energy Electrons Traversing Dilute Gases*, Reviews of Modern Physics, **42, N 2** (1970), 237–271.

[8] L. O.'C. Drury, F. A. Aharonian, and H. J. Völk, *The Gamma-Ray Visibility of Supernova Remnants: a Test of Cosmic Ray Origin*, Astron. and Astrophys., **287** (1994), 959.

[9] E. Fermi, *On the Origin of the Cosmic Radiation*, Phys. Rev. **75** (1949), 1169–1174.

[10] T. Inoue, R. Yamazaki, and S. Inutsuka, *Two-step Acceleration Model of Cosmic Rays at Middle-aged Supernova Remnants: Universality in Secondary Shocks*, The Astrophysical Journal Letters, **723** (2010), L108.

[11] J. Krause, E. Carmona, and I. Reichardt, *Probing Proton Acceleration in W51C with MAGIC*, III FERMI Symposium,, 2011.

[12] D. Perkins, *Particle Astrophysics,*, 2nd ed., p. 237, Oxford University Press, 2009.